Visible Light Photocatalytic Inactivation of Resistant *Escherichia coli* by SiC/g-C_3N_4

[1]Wenming Jiang*, [2]Chaoxia Wang**, [3]Rujira Sukhotu, [1]Shiyang Zhou, [1]Ying Yuan, [1]Le Li, [1]Jingjing Yang
[1]*Chongqing Chemical Industry Vocational College, Chongqing 401228, China.*
[2]*Tianjin Agricultural University, Tianjin 300384, China.*
[3]*Krabi agricultural research and development center, Department of Agriculture, Krabi 81000, Thailand.*
hahajing1229@163.com*

(Received on 31st October 2022, accepted in revised form 30th April 2024)

Summary: SiC/g-C_3N_4 (SCN) was synthesized to inactivated the resistant bacteria; and the binding of SiC to g-C_3N_4 was simply determined by FT-IR. Plasmid pET-28a(+) carrying kanamycin resistance was transformed into the competence of *Escherichia coli* (*E. coli*), and its positive bacteria was used as the object of photocatalytic inactivation. Catalytic conditions were optimized, under which the bactericidal kinetics and reuse of the materials were studied. The photoelectric reaction and light absorption were studied by electrochemical workstation and UV-vis DRS. In addition, potassium dichromate (Cr^{6+}), isopropanol (IPA), methanol (MTA), sodium oxalate ($Na_2C_2O_4$) and 4-hydroxy-2, 2, 6, 6-tetramethylpiperidinyloxy (TEMPOL) were used to study the photocatalytic mechanism. FT-IR results showed that SCN was successfully synthesized, and the positive *E. coli* was obtained. Under optimal inactivation conditions, SCN had good reusability. Photoelectric experiments showed that the photogenerated electrons (e^-) and holes (h^+) were more easily separated, and SCN has a larger spectral absorption range and a lower band gap. According to the kinetic study, SCN and g-C_3N_4 had great advantages in sterilization efficiency. Mechanism study showed that e^-, h^+, hydrogen oxygen radicals ($\cdot OH$) and superoxide radicals ($\cdot O_2^-$) were generated in the photocatalytic process, and $\cdot O_2^-$ played the most important roles in inactivation.

Key words: SiC; g-C_3N_4; photocatalysis; *E. coli.*

Introduction

China is a major producer and consumer of antibiotics, which are widely used in many fields. In high-density aquaculture, a large number of antibiotics are used to inhibit the growth of pathogenic microorganisms, which leads to the accumulation in the sludge at the bottom of the pond. The long-standing antibiotics will induce the breeding of antibiotic resistant bacteria [1], which leads farmers to use new antibiotics, otherwise it will lead to aquaculture loss. Therefore, eliminating pathogenic microorganisms in the water environment without producing resistant bacteria has become one of the main tasks for the water treatment. However, some traditional water sterilization methods have many disadvantages, such as high energy consumption and safety problems [2], which are not conducive to sustainable development. Photocatalysis is a promising technology for inactivating bacteria, which is largely because it is possible to directly use solar energy and drive the inactivation process of microorganisms [3-6]. So far, much efforts have been devoted to design the photocatalysts with high catalytic efficiency, among which TiO_2 was studied the most widely [7-9]. However, application of TiO_2 is adversely affected by its large bandgap energy [10], which is only excited by ultraviolet light accounting for less than 5% of the solar spectrum. Meanwhile, metal oxides [11], sulfides [12], oxynitrides [13] and especially co-catalysts [14] has also been widely studied. The co-catalysts loaded with Pt [15], Ag [16] and Au [17] could enhance the photocatalytic activity due to its excellent electron trapping ability. However, the high cost of use severely limits their large-scale application. For this reason, it is desirable to develop high catalytic activity with low cost. Material g-C_3N_4 that can be simply synthesized by melamine and urea as the precursors is such photocatalyst [18-19]. However, g-C_3N_4 is affected by high electron-hole recombination rate [20], which needs modification to improve its catalytic properties [21-23]. SiC is a relatively common environment-friendly and corrosion-resistant material on the earth, which has an appropriate band gap [24-26]. In previous studies, SCN had the potential of photocatalytic degradation of various organic substances [24, 26-27]. Therefore, its deserved to study whether SCN is effective for the

*To whom all correspondence should be addressed.

inactivation of antibiotic resistance bacteria. In this research project, SCN was synthesized by melamine and SiC, and the composite SCN was used to inactivate antibiotic resistant *E. coli* under natural light. The influence of the addition amount of photocatalyst, PS and initial pH on the inactivation were also considered in this research project. Meanwhile, the sterilization kinetics and reuse rate of the material were studied, which provided some theoretical guidance for the further application of SCN in aquaculture.

Experimental

Transformation

Plasmid pET-28a(+) with the kanamycin resistance gene was transformed to the competence of *E. coli*. The bacterial mixture was spread onto Luria-Bertani (LB) solid medium with the kanamycin concentration of 100 mg/mL to get several single colonies, which was further confirmed by PCR. The positive strains were cultured in LB liquid medium for subsequent experiments.

Materials

β-SiC powder purchased from Xikeboer with size of 4-5 μm was pretreated according to a reference [24]. Graphite phase C3N4 was prepared by thermal polymerization of melamine. In short, 2g of melamine was heated at 550℃ for 2 hours at a heating rate of 5℃/min [14]. SCN was synthesized by SiC and melamine at a mass ratio of 1:50 in according to the method of previous study [24].

Characterization by UV-vis DRS and FT-IR

The UV-visible diffuse reflectance spectrum (UV-vis DRS) was obtained using the UV-visible spectrophotometer (TU-1901, Beijing Pukenye General Instruments Co., Ltd.), and the barium sulfate was used as the reflectance standard. Structures of SCN, g-C_3N_4 and SiC were characterized by a fourier transform infrared spectrometer (FT-IR, Nicolet 670). Photocatalysts were pressed on the potassium bromide (KBr) disk to test the spectra and analyzed by elimination the background of KBr.

Photocurrent measurements

Photocurrent was measured of on an electrochemical workstation (CHI 660D, Shanghai Chen Hua Instrument Company, China), using Pt and saturated calomel electrode as counter and reference electrode, respectively. After cleaning by sonication in ethanol for 30 min, the indium-tin oxide (ITO) glasses were prepared as working electrode. Samples of 10 mg and a drop of 5 wt% nafion solution were dispersed in absolute alcohol, which was dispersed by ultrasonic treatment. Then, catalyst colloid of 100 μL was dispersed on the glass and dried to used.

Bacterial Inactivation

E. coli DH5α with antibiotic resistance was prepared as sterilization target. Bacteria were cultivated in LB liquid medium at 37 °C overnight, and then centrifuged at 4000 rpm for about 15 min. Bacterial precipitation was washed by sterilized physiological saline for three times and re-suspended in a centrifuge tube, the absorbance of which at OD600 was adjust by spectrophotometer to acquire a suitable concentration (10^5-10^6 cfu/mL). The bacterial suspension with photocatalyst was added into 0.9% NaCl solution, which was irradiated in multichannel photochemical reaction device (PCX-50C). Then, the collected samples were diluted with sterile saline and evenly smeared onto LB solid culture medium. The plate was then incubated at 37℃ overnight to determine the sterilization rate. The influence of the addition amount of photocatalyst, PS concentration and initial pH on the inactivation of thallus were considered in this experiment.

Radical trapping

This experiment was carried out by adding individual scavenger in the inactivation test. IPA, MTA, Cr^{6+}, $Na_2C_2O_4$ and TEMPOL were used to capture OH, e^-, SO_4^-, h^+ and O_2^- respectively. The catalytic inactivation without scavenger was regarded as control.

Results and Discussion

Transformation

In order to facilitate experiments, the sampling and photocatalysis were all needed to be exposed to the outside air. In addition, there are various microorganisms in the air. Therefore, in order to prevent the interference of other microorganisms, genetically modified *E. coli* was used as a photocatalytic strain in this project. According to the DNA sequence of plasmid pET-28a(+) (Fig. 1a), primers (For-ACGACGATACCGAAGACAGC; Rev-TGACTGGGTTGAAGGCTCT) were designed for

PCR detection of single colonies. It can be seen from Fig. 1b that the required cloned bands appeared at about 349 bp, which further indicates that the bacteria carrying plasmid pET-28a(+) has been obtained (Fig. 1b, lane 1). After that, the selected positive bacteria were expanded for photocatalytic inactivation experiment.

FT-IR

In previous studies, g-C_3N_4, SiC and SCN had been characterized [24]. When the ratio of SiC to melamine is 1:50, material SCN had good catalytic activity for rhodamine B. Therefore, SCN was prepared by the same proportion, material and synthesis method in this study. FT-IR is a powerful tool for analyzing the structure of matter, which was widely used to analyze and identify substances and study the interactions between molecules. As can be seen from Fig. 2, SiC had characteristic absorption peaks at 809, 834 and 1624 cm^{-1}. Since the absorption peaks at 809 and 834 cm^{-1} were similar in distance and peak value, the absorption curve between 450 and 1062 cm^{-1} was generally wide and gentle. According to the analysis of the characteristic peaks of SiC infrared spectrum [28], the absorption at about 838 cm^{-1} was assigned to the stretching vibration of structure Si-C. Stretching vibration of C-C at 1624 cm^{-1} indicates the existing of slight graphitized carbon. Material g-C_3N_4 has characteristic peaks at 808, 888, 992, 1322 and 1640 cm^{-1}. The absorption peak at 808 cm^{-1} was triazine ring, the peak at 1322 cm^{-1} was aromatic C-N, while the peak at 1640 cm^{-1} was C=N [29]. SCN had obvious characteristic peaks at 809, 887, 990 and 1330 cm^{-1}, which was similar to g-C_3N_4. Due to the influence of SiC, the absorption peak at 888 cm^{-1} almost disappeared, but was strengthened at 990 cm^{-1}, which indicates that a heterojunction was formed between SiC and g-C_3N_4.

Photocatalytic bacterial inactivation

In order to study the sterilization effect of materials, 1000 mg/L SiC, g-C_3N_4 and SCN solutions were prepared with 0.9% physiological saline. SCN of 1000 mg/L in dark and physiological saline without photocatalyst in light were used as control. *E. coli* DH5α with kanamycin resistance was used to evaluate the inactivation performances of SCN. It can be seen that the two controls and SiC basically had no bactericidal effect. SCN and g-C_3N_4 showed the similar trend (Fig.3a). The bactericidal rate increased significantly before 60 min, and then began to increase slowly. At 210 min, the bactericidal rate was all above 90%. Overall, the germicidal effect of SCN was better than that of g-C_3N_4, indicating that SiC could improve the bactericidal effect of g-C_3N_4.

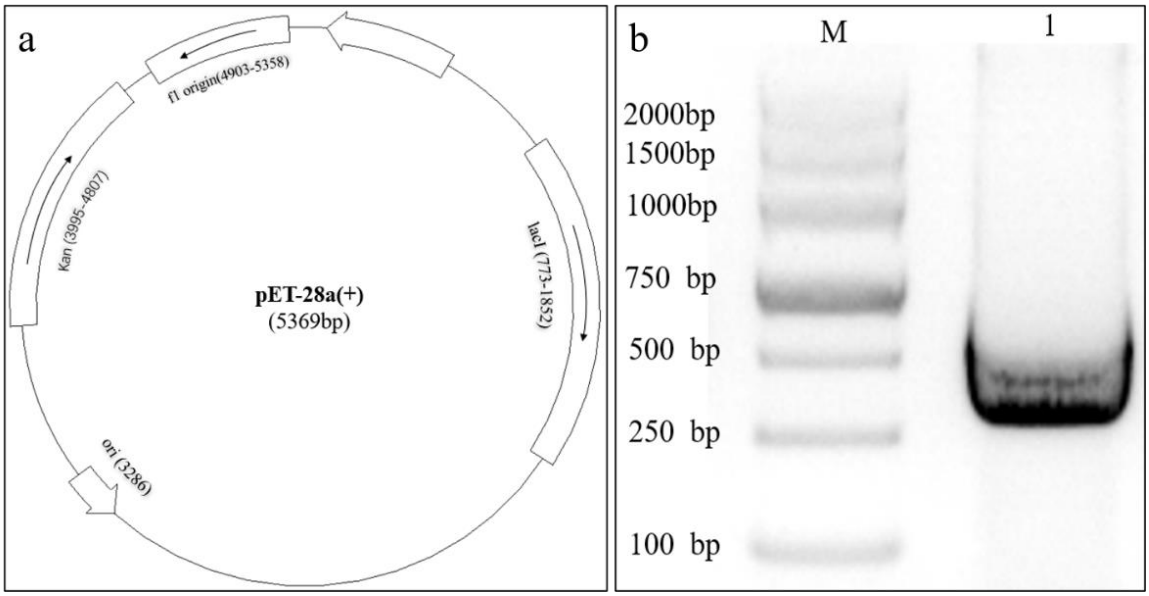

Fig. 1: Plasmid (a) and electrophoresis bands(b).

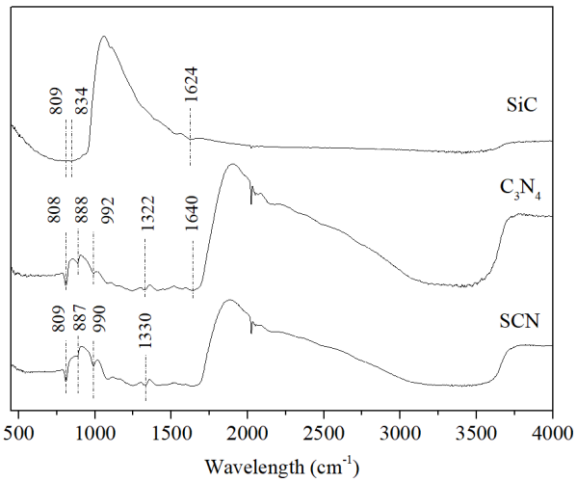

Fig. 2: FT-IR spectrum of SiC, g-C_3N_4 and SCN.

After comparison with SiC and g-C_3N_4 in sterilization, SCN was selected for further study. In order to save the material cost, the effects of different SCN concentrations (200, 400, 600, 800, 1000 mg/L) on the sterilization effect were studied. It can be seen from Fig. 3b that different concentrations of SCN basically showed the same sterilization trend. The germicidal curves of various concentrations were clustered together and there was no significant difference in germicidal efficacy. That is, the bactericidal effect of SCN did not significantly increase when the concentration was more than 200 mg/L. With the increase of g-C_3N_4 concentration, the turbidity increased linearly (Fig. 3c). Therefore, there was no significant change in the bactericidal effect, which may be due to the high turbidity hindering the catalysis of light on SCN.

PS can effectively suppress the undesired recombination of electrons and holes, which could improve the photocatalytic activity [30]. Because the high recombination of photoexcited carriers of g-C_3N_4, PS was selected to improve the catalytic activity of SCN with the concentration of 200 mg/L that was screened by the previous experiments. Although PS can improve the catalytic activity, the higher concentration will cause secondary pollution as it is water soluble. Therefore, in this experiment, the effect of different PS concentrations (0.2, 0.5, 1, 2, 4 mM) on the photocatalysis of SCN was studied to reduce its usage amount. Since PS has catalytic activity, 1 mM concentration of it without photocatalyst was used as a sample. As can be seen from Fig. 3d, the sterilization efficiency of SCN was higher with the increase of PS concentration. The samples with PS concentration of 4, 2 and 1 mM were completely sterilized at 20, 30 and 50 min respectively, while the samples with PS concentration of 0.5 and 0.2 mM were almost completely sterilized at 80 min. PS could sterilize separately under visible light in the absence of photocatalyst, which is consistent with the previous study [31]. Compared with the previous studies, the combined bactericidal effect of SCN and 1 mM PS was significantly better than that of SCN and PS alone, which indicates that there was synergy between them.

Considering the cost and sterilization efficiency, 1 mM PS was selected for the followed experiment. pH has certain influence on sterilization, therefore, the variation of pH in the range of 3.0-11.0 was studied on the bacterial inactivation efficiency. As can be seen from Fig. 3e, the sterilization effect was the best when the pH value was 3, and the sterilization can be completed in 10 min. The sterilization effect of pH 11 and 5 was relatively better than 9 and 7, and it could be completed within 20 min. In all pH comparison experiments, the bactericidal effect was the lowest at pH 7, which was different from the previous study [31]. In general, acidic and alkaline pH had better bactericidal effect than neutral pH, and acidic pH was better than alkaline pH, suggesting that acidic pH could improve the disinfection activity. This may be due to that the charge layer on the surface of *E. coli* was destroyed at non neutral pH environment, especially in acidic pH, which made the bacteria more vulnerable to free radicals.

Because the sterilization effect at pH 5 was relatively better and the reagent consumption in the pH adjustment was less, it was selected for the next optimization experiment. Since the pollutants of water dissolved are more difficult to treat than the insoluble, the addition amount of PS was further optimized here to reduce the addition amount of water-soluble reagent. It can be seen from Fig. 3f that the sterilization effect of the sample with PS concentration of 0.5 mM was the best, and it was almost 100% inactivated in 50 min. Overall, the inactivation rate of 200 mg/L SCN with different concentrations of PS (0.5, 0.25 and 0.1 mM) increased rapidly at the beginning, and the gap between them became larger; but after 20 min, all the inactivation rates increased slowly, and the difference between them decreased slowly. Therefore, in the range of 0.1-0.5 mM PS, the effect of SCN on the bactericidal effect may be greater than that of PS.

Application and inactivation kinetics

The regeneration and reuse of photocatalysts are very important for practical application. To evaluate the recycling ability of SCN photocatalyst, four cycle experiments were carried out at pH 5 with SCN and PS

concentration of 200 mg/L and 0.1 mM respectively. Results as shown in Fig. 4a, the sterilization rate of SCN against *E. coli* remained above 94% after repeated use for the third time, suggesting the composite material can be reused for many times without activity deterioration. Therefore, the repeated use of SCN can reduce the material cost, which lays a foundation for its practical application.

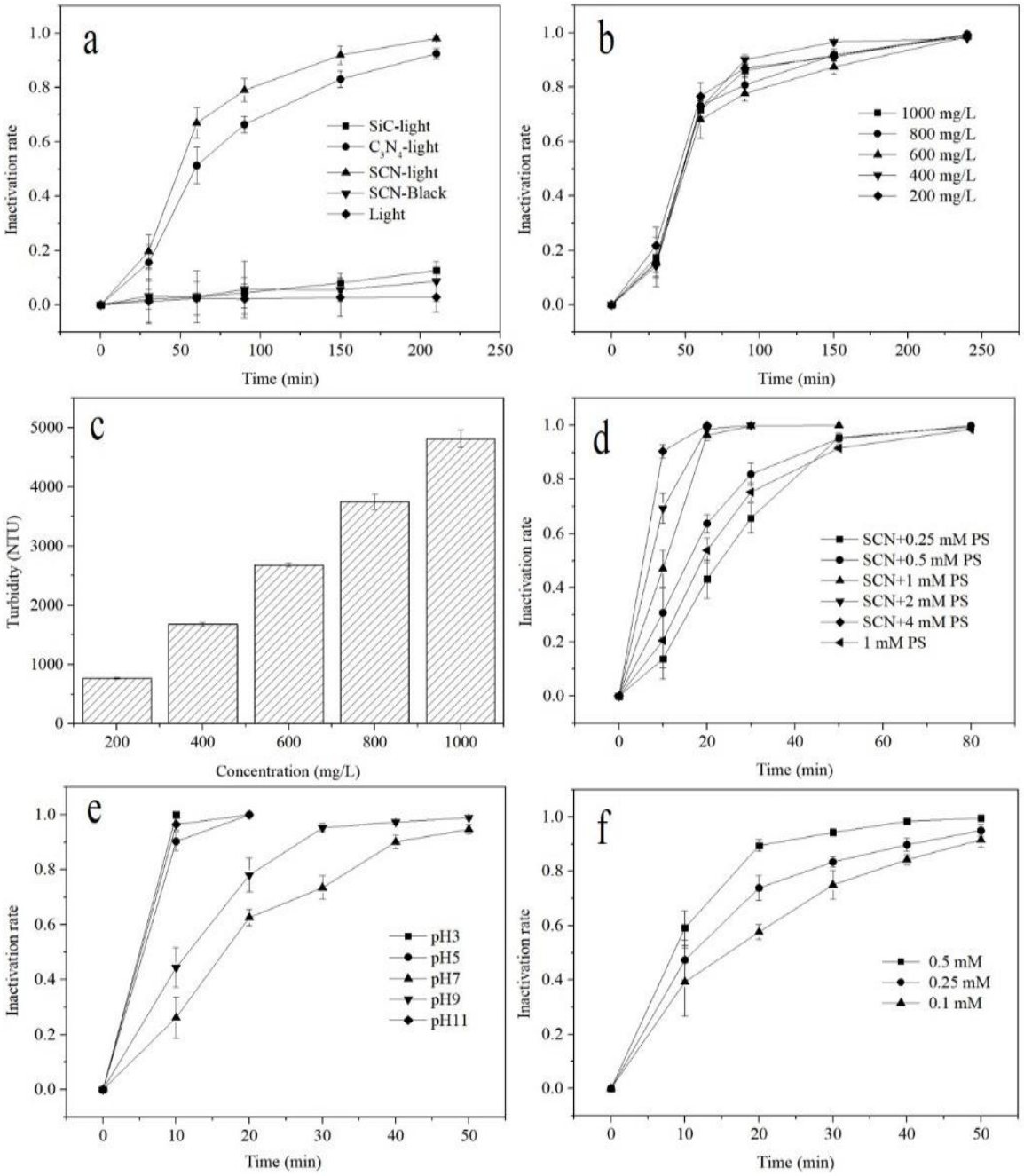

Fig. 3: (a) Comparison of inactivation effects of SCN, SiC and g-C_3N_4; (b) Effect of SCN addition on inactivation; (c) Turbidity of different SCN addition; (d) Effect of different concentrations of PS on inactivation; (e) Effect of pH on inactivation; (f) Further optimization of PS concentration.

The inactivation kinetics was study by the decay of viability according to the model [32] and modified by Wang et al (Eq. 1) [33]. N_0 and N_t were the survival number of *E. coli* at initial time and reaction time respectively; N_r was the residual number of the *E. coli* and K_m represented the inactivation rate. Eq. 1 was transformed to form Eq. 2 for calculation.

$$N_t = (N_0-N_r) \times \exp(-k_m \times t) + N_r \quad (01)$$

$$\mathrm{Ln} \left(\frac{N_0-N_r}{N_t-N_r} \right) = k_m \cdot t \quad (02)$$

SCN sample of 200 mg/L with 0.1 mM PS was used for photocatalytic sterilization at pH 5, and g-C_3N_4 with the same addition amount, PS concentration and pH was also carried out to compare with the previous study (Fig. 4b) [33]. As can be seen from Fig. 4c, the results were fitted with the Eq. 2 (SCN, R^2=0.9923; g-C_3N_4, R^2=0.9736). The K_m value of SCN was 0.0533 min^{-1} and slightly higher than that (0.0509 min^{-1}) of g-C_3N_4, which was also indicated that SiC enhanced the photocatalytic bacterial inactivation efficiency of g-C_3N_4. Compared with 0.570×10^{-2} min^{-1} in the comparison document, the k_m value of g-C_3N_4 in this study was about 9 times of it, which was mainly due to the difference in experimental conditions. In addition, the SCN also exhibits at least 15 times higher than that of CNP.

The difference between the bactericidal rates of SCN and g-C_3N_4 under the same conditions was not large, so electrochemical workstation and UV-vis DRS were used to detect the photoelectric response and spectral absorption of the three materials respectively. It can be seen that under visible light irradiation, all three materials could generate stable photocurrent (Fig. 5a). The photocurrent intensity produced by SCN was higher than that of pure SiC and g-C_3N_4 materials, which indicates that a heterojunction was formed between SiC and g-C_3N_4 and was conducive to the separation of photogenerated electrons and holes. The comparison of UV-vis DRS absorption spectra of photocatalysts is shown in Fig. 5b. All three materials can be excited by visible light. The absorption edge of SCN and g-C_3N_4 was at 460 and 452 nm respectively, indicating that SCN had a greater absorption over the entire wavelength range. After calculation, the results of band gap are shown in Fig. 5c. The band gap of SCN and g-C_3N_4 was 2.80 and 2.82 eV respectively, suggesting that the separation efficiency of electrons and holes had been improved after the loading of SiC. But on the whole, the difference between SCN and g-C_3N_4 in absorption edge and band gap was not large.

Inactivation mechanism

A scavenging study was performed to illuminate the photocatalytic mechanism. The scavengers of Cr^{6+}, IPA, MTA, $Na_2C_2O_4$, and TEMPOL with concentration of 0.05, 0.5, 1.0, 0.5 and 0.5 mM was used in this process [30, 34]. As shown in the Fig. 6a, there was no obvious effect on the inactivation efficiency with the addition of Cr^{6+} and MTA, suggesting that e^- and $\cdot SO_4^-$ were not the main species in the process of vitality decline. It was found that the addition of IPA, $Na_2C_2O_4$ and TEMPOL could inhibit the inactivation efficiency, which mean that the main species were $\cdot OH$, $\cdot O_2^-$, and h^+.

Since the photogenerated holes were captured by sodium oxalate, photogenerated electrons were bound to accompany their generation. However, the electrons were hardly captured by Cr^{6+}. Therefore, the free electrons may participate in other processes or be trapped by other stronger electron trapping agents. In addition, methanol did not capture $\cdot SO_4^-$, and PS was an electron trapping agent [30], therefore, electrons may react with PS or $\cdot SO_4^-$. Because the bactericidal rate decreased after adding IPA, $\cdot OH$ radicals were generated in the photocatalytic process; However, methanol did not capture $\cdot OH$, but IPA did. This may be because the substances produced under the catalytic conditions had greater inhibition on MTA than IPA. The effect of adding TEMPOL was greater than that of IPA, which may be due to the amount of $\cdot O_2^-$ produced in the photocatalytic process was more than $\cdot OH$, or the generation of $\cdot OH$ is relatively more difficult. In addition, according to the positions of conduction band and valence band of SiC (CB -0.23 eV, VB 2.16 eV) and g-C_3N_4 (CB, -1.12 eV; VB, 1.54 eV), hydrogen was generated during the catalytic process. Based on the above analysis, the mechanisms of the inactivation system may experience the following reactions (Eq. 3 & 4), and the schematic diagram was showed as Fig. 6b.

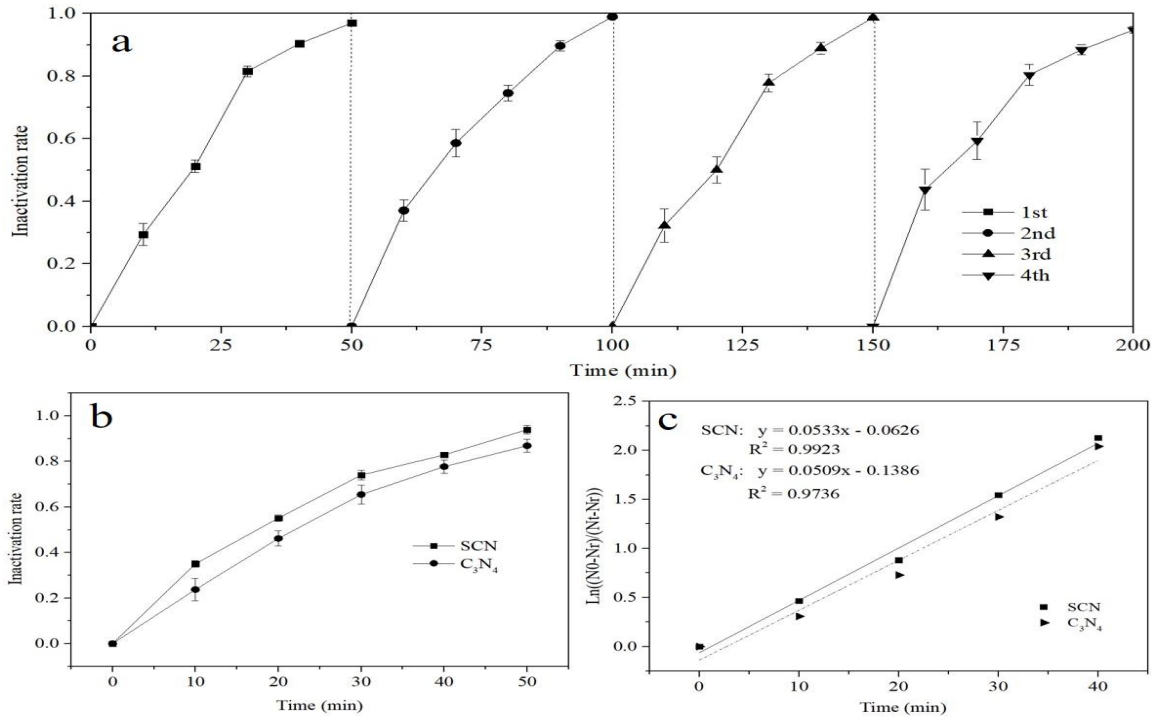

Fig. 4: (a) Reuse of SCN; Inactivation effect (b) and inactivation kinetics curve(c) under optimal conditions.

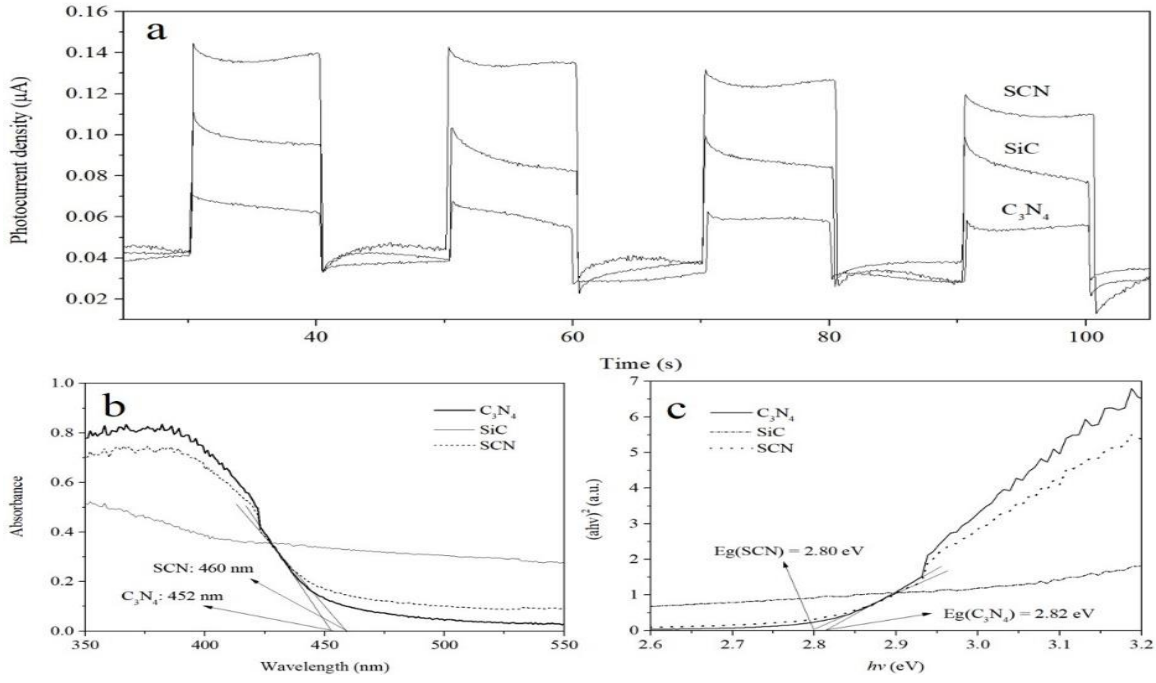

Fig. 5: Photocurrent density (a), spectral absorption range(b) and band gap(c) of materials.

$$S_2O_8^{2-} + 2H_2O + e^- \rightarrow 2\cdot SO_4^- + 2H_2 + \cdot O_2^- \quad (03)$$

$$\cdot SO_4^- + 2e^- + 2H_2O \rightarrow SO_4^{2-} + OH^- + \cdot OH + H_2 \quad 4$$

First, PS hydrolyzed and generated $S_2O_8^{2-}$ ions. After obtaining the energy of one electron, $S_2O_8^{2-}$ with H_2O generate two $\cdot SO_4^-$ radicals, one $\cdot O_2^-$ and two H_2. After obtaining two electron energies, $\cdot SO_4^-$ radical with two H_2O generated SO_4^{2-}, OH^-, $\cdot OH$ radical and H_2. Since $\cdot O_2^-$ was produced earlier than $\cdot OH$ in the whole reaction process and required less energy, $\cdot O_2^-$ played a greater role in sterilization. OH^- was formed during the reaction, and its inhibition on methanol was probably greater than that of isopropanol in the capture of $\cdot OH$; Acidic conditions can also accelerate the rightward progression of Eq. 4.

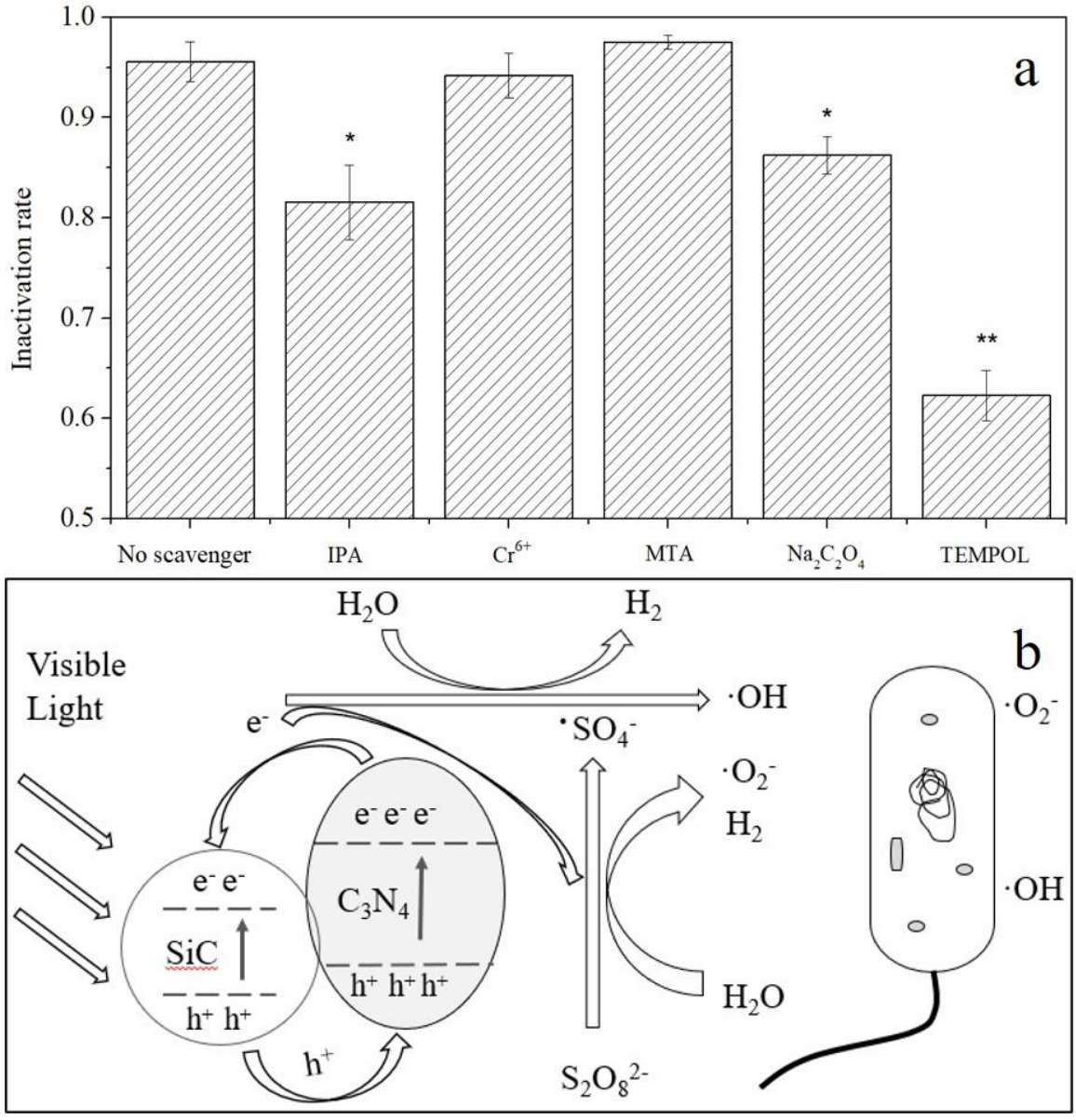

Fig. 6: Photocatalytic inactivation efficiencies with different scavengers (a) and Schematic illustration of inactivation mechanism(b).

Conclusions

Due to the use of a large quantity of antibiotics in aquaculture, many resistant bacteria have been screened out and caused huge losses to the aquaculture every year. In this study, SCN was synthesized to inactivate the resistant bacteria. The composites were characterized by FT-IR, and it was confirmed that SiC and g-C_3N_4 were bonded together. In order to facilitate the experimental operation and ensure the accuracy of the experiment, the plasmid pET-28a(+) carrying kanamycin resistance was transformed into the competence of *E. coli*, and the positive bacteria screened by kanamycin and PCR were used as the target of photocatalytic inactivation. In the catalytic experiments, the addition amount of SCN, PS concentration and pH value were optimized to improve the photocatalytic effect of SCN. Results showed that the optimal inactivation conditions were: SCN 200 mg/L, PS 0.1 mm and pH 5, under which SCN had a good reusability. Transient photocurrent response was analyzed by electrochemical workstation, which showed that the e^- and h^+ of SCN were easier to separate; after analyzing the UV-vis DRS detection results, SCN has a larger spectral absorption range and a narrower band gap; however, the above difference between SCN and g-C_3N_4 were not obvious. In addition, Cr^{6+}, IPA, MTA, $Na_2C_2O_4$ and TEMPOL were used to study the photocatalytic mechanism. The results showed that e^-, h^+, ·OH and $\cdot O_2^-$ were produced in the photocatalytic process, and $\cdot O_2^-$ played the main roles in the inactivation. In conclusion, this study provides the optimum experimental scheme for SCN inactivating resistant bacteria in aquaculture.

Acknowledgements

This work was supported by the Science and Technology Research Program of Chongqing Municipal Education Commission (Grant No. KJQN202204503).

References

1. Zhao Y., Wang Q., Liu H., et al. High-throughput sequencing of 16S r RNA amplicons characterizes gut microbiota shift of juvenile sea cucumber *Apostichopus japonicus* feeding with three antibiotics[J]. Journal of Oceanology and Limnology, **37,** 248 (2019).
2. Zhang D., Li G., Yu J.C. Inorganic materials for photocatalytic water disinfection [J]. Journal of Materials Chemistry, **20,** 4529 (2010).
3. Anwar A., Khalid S., Perveen S., et al. Synthesis of 4-(dimethylamino) pyridine propylthioacetate coated gold nanoparticles and their antibacterial and photophysical activity[J]. Journal of nanobiotechnology, **16,** 1 (2018).
4. Wang W., Yu J.C., Xia D., et al. Graphene and g-C_3N_4 nanosheets cowrapped elemental α-sulfur as a novel metal-free heterojunction photocatalyst for bacterial inactivation under visible-light[J]. Environmental science & technology, **47,** 8724 (2013).
5. Aqeel Y., Siddiqui R., Anwar A., et al. Photochemotherapeutic strategy against *Acanthamoeba* infections [J]. Antimicrobial Agents and Chemotherapy, **59,** 3031 (2015).
6. Huang J., Li D., Li R., et al. An efficient metal-free phosphorus and oxygen co-doped g-C_3N_4 photocatalyst with enhanced visible light photocatalytic activity for the degradation of fluoroquinolone antibiotics [J]. Chemical Engineering Journal, **374**: 242-253 (2019).
7. Liu X., Liu X., Shan J., et al. Synthesis of amorphous mesoporous TiO_2-SiO_2 and its excellent catalytic performance in oxidative desulfurization[J]. Inorganic Chemistry Communications, , **123**:108336 (2020).
8. Liu G., Wang L., Hu Y., et al. Enhanced Catalytic Effect of TiO_2@rGO Synthesized by One-pot Ethylene Glycol-assisted Solvothermal Method for MgH2[J]. *Journal of Alloys and Compounds,* , **881,** 160644 (2021).
9. Junkaew A., Ehara M., Huang L., et al. Facet-Dependent Catalytic Activity of Anatase TiO_2 for the Selective Catalytic Reduction of NO with NH3: A Dispersion-Corrected Density Functional Theory Study [J]. Applied Catalysis A General, 118250 (2021).
10. Han B., Hu Y.H. In-situ FTIR Investigation on TiO2 reduction [J]. American Chemical Society, Division of Fuel Chemistry, Preprints, **58,** 294 (2013).
11. Chen W., Hou X., Shi X., et al. Two-dimensional Janus transition metal oxides and chalcogenides: multifunctional properties for photocatalysts, electronics, and energy conversion [J]. ACS applied materials & interfaces, **10,** 35289 (2018).
12. Maheu C., Puzenat E., Geantet C., et al. Titania-Supported transition metals sulfides as photocatalysts for hydrogen production from propan-2-ol and methanol[J]. International journal of hydrogen energy, , **44,** 18038 (2019).
13. Hu C.C., Teng H. Gallium Oxynitride Photocatalysts Synthesized from $Ga(OH)_3$ for Water Splitting under Visible Light Irradiation[J]. Journal of Physical Chemistry C, , **114**: 20100-20106 (2010).
14. Wang W., Gu W., Li G., et al. Few-layered tungsten selenide as a co-catalyst for visible-light-driven photocatalytic production of hydrogen peroxide for bacterial inactivation[J]. Environmental Science:

Nano, 7, 3877-3887 (2020).
15. Lin F., Wang D., Jiang Z., et al. Photocatalytic oxidation of thiophene on BiVO4 with dual co-catalysts Pt and RuO2 under visible light irradiation using molecular oxygen as oxidant[J]. Energy and Environmental Science, **5,** 6400 (2012).
16. Hu C., Peng T., Hu X., et al. Plasmon-induced photodegradation of toxic pollutants with Ag-AgI/Al_2O_3 under visible-light irradiation[J]. Journal of the American Chemical Society, 132, 857 (2010).
17. Yan W., Overbury S.H., Dai S., et al. Preparation of highly active silica-supported Au catalysts for CO oxidation by a solution-based technique[J]. Journal of Physical Chemistry B, 2006, **110,** 10842 (2010).
18. Liang J., Jing C., Wang J., et al. Photocatalytic Reduction of Cr (VI) over g-C_3N_4 Photocatalysts Synthesized by Different Precursors[J]. Molecules, , **26,** 7054 (2021).
19. Ong W.J., Tan L.L., Ng Y.H., et al. Graphitic carbon nitride (g-C_3N_4)-based photocatalysts for artificial photosynthesis and environmental remediation: are we a step closer to achieving sustainability?[J]. Chemical reviews, **116**, 7159 (2016).
20. Chen S., Hu Y., Meng S., et al. Study on the separation mechanisms of photogenerated electrons and holes for composite photocatalysts g- C_3N_4-WO_3[J]. Applied Catalysis B: Environmental, **150**: 564-573 (2014).
21. Chen X., Zhang J., Fu X., et al. Fe-g-C_3N_4-Catalyzed Oxidation of Benzene to Phenol Using Hydrogen Peroxide and Visible Light[J]. Journal of the American Chemical Society, **131**: 11658 (2009).
22. Ge L., Han C., Xiao X., et al. Synthesis and characterization of composite visible light active photocatalysts MoS_2-g-C_3N_4 with enhanced hydrogen evolution activity[J]. International Journal of Hydrogen Energy, **38,** 6960 (2013).
23. Le S., Jiang T., Li Y., et al. Highly efficient visible-light-driven mesoporous graphitic carbon nitride/ZnO nanocomposite photocatalysts[J]. Applied Catalysis B: Environmental, **200**: 601 (2017).
24. Yang J., Peng Y., Yang B., et al. Enhanced photocatalytic degradation of Rhodamine B over metal-free SiC/C_3N_4 heterostructure under visible light irradiation[J]. Materials Research Express, **5**: 085511 (2018).
25. Wu X.L., Xiong S.J., Zhu J., et al. Identification of surface structures on 3C-SiC nanocrystals with hydrogen and hydroxyl bonding by photoluminescence[J]. Nano letters, **9**, 4053 (2009).
26. Xu H., Gan Z., Zhou W., et al. A metal-free 3C-SiC/g-C_3N_4 composite with enhanced visible light photocatalytic activity[J]. RSC advances, **7**: 40028 (2017).
27. Zhu H., Yang B., Yang J., et al. Persulfate-enhanced degradation of ciprofloxacin with SiC/g-C_3N_4 photocatalyst under visible light irradiation[J]. Chemosphere, **276,** 130217 (2021).
28. Zhan H., Zhang N., Wu D., et al. Controlled synthesis of β-SiC with a novel microwave sintering method[J]. Materials Letters, **255**, 126586 (2019).
29. Ren Y., Li Y., Wu X., et al. S-scheme Sb_2WO_6/g-C_3N_4 photocatalysts with enhanced visible-light-induced photocatalytic NO oxidation performance[J]. Chinese Journal of Catalysis, **42**: 69-77 (2021).
30. Wang W., Wang H., Li G., et al. Visible light activation of persulfate by magnetic hydrochar for bacterial inactivation: Efficiency, recyclability and mechanisms[J]. Water research, **176**: 115746 (2020).
31. Wang W., Wang H., Li G., et al. Catalyst-free activation of persulfate by visible light for water disinfection: efficiency and mechanisms[J]. Water research, 157: 106 (2019).
32. Geeraerd A.H., Herremans C.H., Van Impe J.F. Structural model requirements to describe microbial inactivation during a mild heat treatment[J]. International journal of food microbiology, **59,** 185 (2000).
33. Wang W., Li G., An T., et al. Photocatalytic hydrogen evolution and bacterial inactivation utilizing sonochemical-synthesized g-C_3N_4/red phosphorus hybrid nanosheets as a wide-spectral-responsive photocatalyst: the role of type I band alignment [J]. Applied Catalysis B: Environmental, , 238: 126 (2018).
34. Gu W., Wang W., Li G., et al. Microwave-assisted synthesis of defective tungsten trioxide for photocatalytic bacterial inactivation: Role of the oxygen vacancy[J]. Chinese Journal of Catalysis, , **41,** 1488 (2020).